Preparation and characterization of thermoplastic vulcanizate/silica nanocomposites

2 AUTHORS, INCLUDING:

Tzong-Ming Wu
National Chung Hsing University
123 PUBLICATIONS **2,461** CITATIONS

Preparation and Characterization of Thermoplastic Vulcanizate/Silica Nanocomposites

Tzong-Ming Wu, Mu-Shun Chu

Department of Material Science and Engineering, National Chung Hsing University, 250 Kuo Kuang Road, Taichung, Taiwan 402

ABSTRACT: This article describes the preparation, characterization, and properties of thermoplastic vulcanizate (TPV)/silica nanocomposites. The nanocomposites were prepared by the melt blending of TPV and maleic anhydride grafted polypropylene (mPP) into organically modified SiO_2 (m-SiO_2), treated with *n*-hexadecyl trimethylammonium bromide as a grafting agent for TPV during the melt mixing. The thermal stability and storage modulus of the 1 wt % m-SiO_2 containing TPV/mPP/m-SiO_2 nanocomposite were higher than those of pristine TPV. The most important observation was obtained from dynamic mechanical analysis, which revealed that the glass-transition temperature of the polypropylene phase of the nanocomposites increased (in comparison with that of virgin TPV), whereas the ethylene–propylene–diene monomer phase remained almost the same. The adhesion strength between the TPV/mPP/m-SiO_2 nanocomposites and steel also increased with increasing m-SiO_2 content. © 2005 Wiley Periodicals, Inc. J Appl Polym Sci 98: 2058–2063, 2005

Key words: adhesion; nanocomposites; thermoplastics

INTRODUCTION

A large number of inorganic materials, such as glass fiber, talc, silica, calcium carbonate, and clay minerals, have been successfully used as additives to improve the strength of polymers. The enhancement of the mechanical property significantly depends on many factors, including the aspect ratio of the fillers, their degree of dispersion and orientation in the polymer matrix, and the adhesion of the interface between the filler and polymer matrix. Polymer/nanoparticle composites exhibit excellent thermal and mechanical properties that are synergistically derived from organic and inorganic components.[1–8]

Thermoplastic elastomers based on blends of uncured ethylene–propylene–diene monomer (EPDM) rubber and polypropylene (PP) are called *thermoplastic polyolefins* (TPOs), whereas blends of PP and dynamically vulcanized EPDM rubber are called *thermoplastic vulcanizates* (TPVs).[9–12] Both TPOs and TPVs contain good mechanical, elastic, processing, and recycling properties and have been widely used in industry to replace conventional crosslinked rubbery materials. In a number of industrial applications such as automotive parts, building materials, and commodity products, the functional and styling needs require that

TPOs and TPVs easily adhere to other materials. However, TPOs and TPVs consist of dispersions of EPDM rubber in a PP matrix, both of which have a low surface energy because of their nonpolar nature and are difficult to bond. Therefore, there is very little information available regarding TPO-based and TPV-based nanocomposites.[13,14]

In this study, we report on the preparation, characterization, and properties of a TPV/silica (SiO_2) nanocomposite. The properties of fabricated TPV/SiO_2 nanocomposites depend on the successful dispersion of SiO_2 into the TPV-based matrix. Because of the absence of polar groups on its backbone, it was not thought that a homogeneous dispersion of SiO_2 in the TPV matrix would be realized. To improve the dispersibility of the SiO_2 nanoparticle, a surface treatment of SiO_2 and bulk grafting or compounding of TPV with other polar constituents such as maleic anhydride can be used to improve the interfacial adhesion between SiO_2 and TPV. Therefore, SiO_2 is first treated with *n*-hexadecyl trimethylammonium bromide (CTAB) and is then designated *m-SiO_2*; this treatment can improve the chemical interaction between SiO_2 and TPV. The modified surfaces are characterized by Fourier transform infrared (FTIR) spectroscopy and transmission electron microscopy. The CTAB-treated SiO_2 is then melt-blended with TPV in the presence of maleic anhydride grafted polypropylene (mPP), which acts as a functionalized compatibilizer. During melt blending, CTAB and mPP will tether themselves onto the TPV backbone by a grafting reaction. The strong interaction caused by the grafting

TABLE I
Compositions of Various Samples

Sample	TPV (g)	CTAB-treated SiO_2 (g)	mPP (g)
TPV	50	—	—
TVS	49	1	—
TVSm1	48	1	1
TVSm3	46	1	3
TVSm5	44	1	5

reaction improves the dispersion of silica in the TPV matrix. Because TPV contains a semicrystalline polymer, PP, the final properties of the nanocomposites are critically related to the crystalline features and behaviors of PP. Therefore, it is necessary to characterize the microstructure and properties of TPV/mPP/m-SiO_2 nanocomposites, especially the adhesion properties of fabricated nanocomposites obtained by the peeling test method.

EXPERIMENTAL

Preparation of the TPV/mPP/m-SiO_2 nanocomposites

The TPV Santoprene used in this study was purchased from Advance Elastomer Systems (Akron, OH) with a specific gravity of 0.97 and a hardness of 80A. Silica nanoparticles with a diameter of 40 nm were used as the dispersed phase to improve the properties of Santoprene. The surface of silica was treated with 25 wt % CTAB cations in an aqueous solution at 60°C for 2 h to improve the interaction between TPV and SiO_2 (designated m-SiO_2). m-SiO_2 was then precipitated with an excess amount of deionized water and dried at 100°C for 12 h in vacuo. The TPV/mPP/m-SiO_2 nanocomposites were prepared by a melt-direct intercalation process with surface-treated SiO_2, mPP, and TPV at 200°C in a Haake rheocorder for 10 min. The mixing formulations and their sample codes are shown in Table I. The TVP/mPP/m-SiO_2 nanocomposites, such as TVS, TVSm1, TVSm3, and TVSm5, containing 1 wt % m-SiO_2 nanoparticles had various mPP contents.

Characterization

FTIR spectroscopy was used to characterize the structure of the TPV/mPP/m-SiO_2 nanocomposites. FTIR spectra were recorded on a PerkinElmer Paragon 500 FTIR. The final spectrum presented is an average of three spectra recorded at different regions over the entire range of the sample. X-ray $\theta/2\theta$ diffraction scans of these specimens were obtained with a Rigaku III 3-kW diffractometer equipped with Ni-filtered Cu Kα radiation in the reflection mode. An ultrathin section of the TPV/mPP/m-SiO_2 film with a thickness of approximate 50 nm was prepared with an ultramicrotome equipped with a diamond knife. Transmission

electron microscopy was carried out with a JOEL transmission electron microscope with an acceleration voltage of 120 keV. Because of the high electron density difference between the clay and polymer matrix, staining of the samples was not necessary.

A thermal analysis of the samples was performed with a PerkinElmer Pyris Diamond differential scanning calorimeter calibrated with indium, and all experiments were carried out under a nitrogen atmosphere. All specimens were weighed in the range of 5–6 mg. The thermal stability of the samples was conducted with a PerkinElmer TGA 7 series apparatus with a heating rate of 10°C/min under a nitrogen atmosphere. DMA experiments were performed on a PerkinElmer DMA 7e apparatus equipped with a film tension clamp. The instrument was programmed to measure the storage modulus over the range of −90 to 80°C at a heating rate of 5°C/min and at a constant frequency of 1 Hz. Calibrations for force, mass, position, and temperature were made in accordance with PerkinElmer procedures. The specimen films were cut with length-to-width ratios greater than 6 to guarantee that the uniform strain was well within the linear viscoelastic region of the samples and the collected data were reproducible. The tensile strength and elongation at break were measured with an Instron tensile tester on an ASTM dog-bone test piece tested up to the fracture at the crosshead speed of 1 mm/min (three specimens were tested for each sample). The peeling test was carried out with specimens having peel adhesion measurements of 20 mm × 24 mm. The specimens were applied to stainless steel and pressed with a 2-kg compressor. The TPV/mPP/m-SiO_2 and stainless steel joints were stored at room temperature for 48 h, and peel adhesion in the 180 direction was measured at a peel rate of 5 mm/min at room temperature with an Instron-type adhesion tester.

RESULTS AND DISCUSSION

Surface modification of SiO_2

Because of the incompatibility between hydrophobic polymers and inorganic SiO_2 nanoparticles, the modification of SiO_2 into organophobic characteristics is a critical stage in the preparation of organic/inorganic nanocomposites. Figure 1 shows the FTIR spectrum of SiO_2 and m-SiO_2 treated by CTAB. The spectrum of untreated SiO_2 shows intensive bands at 1120 and 470 cm^{-1} assigned to the Si—O stretching vibration and Si—O—Si bending vibration, respectively. For the CTAB-treated SiO_2, several peaks around 3028, 2955, and 699 cm^{-1} corresponding to the C—H stretching mode of the alkane group in CTAB have been obtained.[15] This result indicates that CTAB successfully grafted onto SiO_2.

Figure 2 shows transmission electron microscopy micrographs of SiO_2 and m-SiO_2, in which the dark
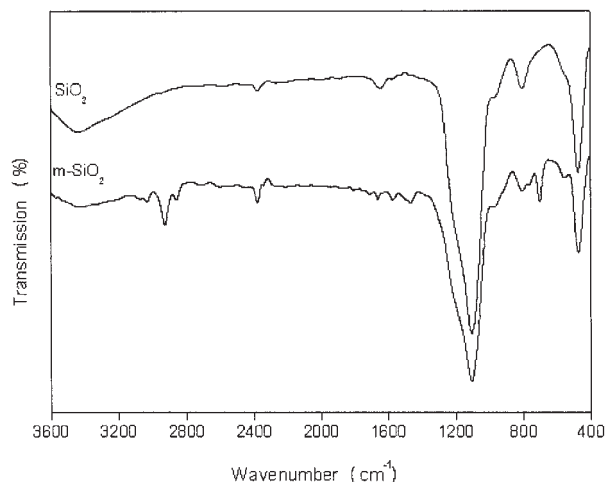
Figure 1   FTIR spectra for SiO_2 and m-SiO_2.

Figure 3   X-ray diffractometer scans for (a) TPV, (b) TVS, (c) TVSm1, (d) TVSm3, and (e) TVSm5 nanocomposites after they were hot-pressed into thin films and then immediately cooled to room temperature at a cooling rate of 20°C/min.

spot represents the distribution of SiO_2. The images of SiO_2 are aggregated together, and the m-SiO_2 particles are well dispersed. Therefore, the results demonstrate that most of the m-SiO_2 particles are randomly distributed in the system.

Microstructural analysis of the TPV/mPP/m-SiO_2 nanocomposites

Figure 3 shows the X-ray diffraction scans of neat TPV and TPV/mPP/m-SiO_2 nanocomposites after they were hot-pressed into thin films at 200°C and then immediately cooled to room temperature at a cooling rate of 20°C/min. All the X-ray diffraction data show
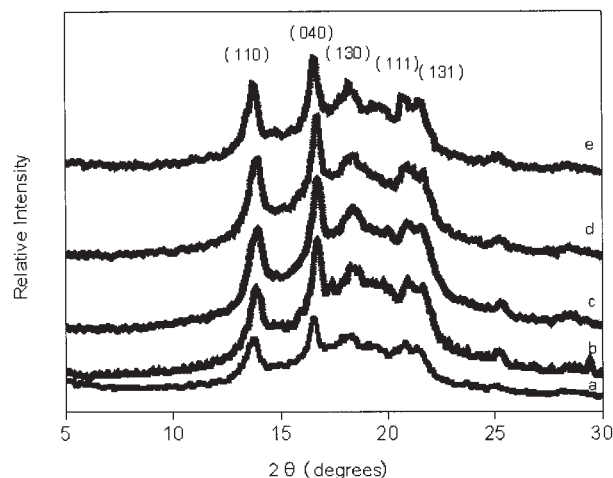
several α-crystalline peaks of (110), (040), (130), (111), and (131) planes ($2\theta \propto$ 14.0, 16.8, 18.5, 21.2, and 21.8°, respectively) and no obvious difference between TPV and TPV/mPP/m-SiO_2 nanocomposites, except for the TVS nanocomposites. The X-ray diffraction data of the TVS nanocomposites show the presence of a mixture of α-crystalline peaks at $2\theta \propto$ 14.0, 16.8, 18.5, 21.2, and 22.0° and traces of a β-crystalline peak at $2\theta \propto$ 16.0°, corresponding to the (300) plane. This result indicates that the addition of 1 wt % m-SiO_2 does slightly affect the crystal structure of the TPV matrix
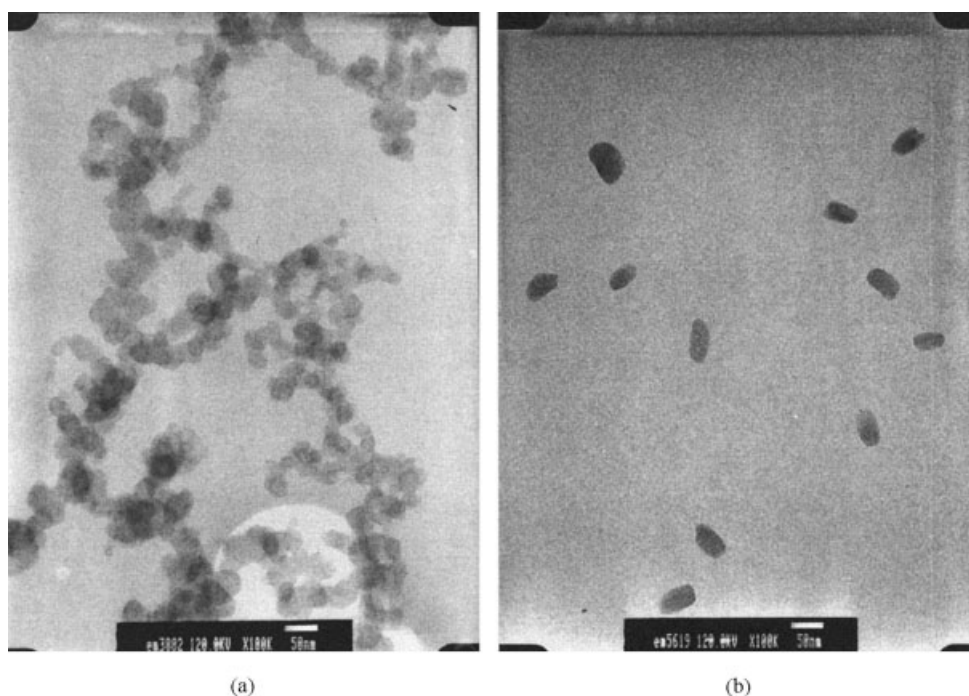

Figure 2   Transmission electron microscopy micrographs of (a) untreated SiO_2 and (b) m-SiO_2.
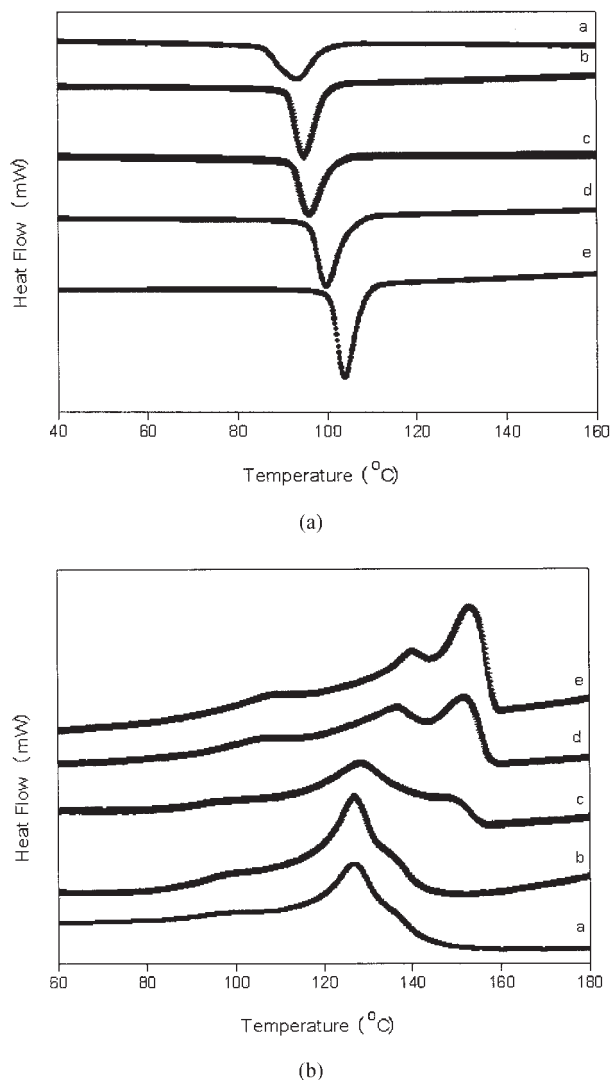
(a)

(b)

Figure 4 (a) DSC cooling scans and (b) DSC second heating scans for (a) TPV, (b) TVS, (c) TVSm1, (d) TVSm3 and (e) TVSm5 nanocomposites.

and could induce the heterogeneous nucleation of the β-crystalline form. The β-crystalline form disappears with the addition of various amounts of functionalized compatibilizer mPP into the system. Figure 4(a) presents the differential scanning calorimetry (DSC) cooling curves of TPV and TPV/mPP/m-SiO$_2$ nanocomposites. The crystallization peak temperatures of the TPV/mPP/m-SiO$_2$ nanocomposites slightly increase with the addition of 1 wt % m-SiO$_2$. The DSC results clearly show that the addition of a small amount of m-SiO$_2$ to the TPV matrix results in an increase in the crystallization temperature (T_c) of the polymer matrix. The observed effect can also be explained by the assumption that m-SiO$_2$ acts as an efficient nucleating agent for the crystallization of the TPV matrix. With the addition of various amounts of mPP into the system, T_c's further increase as the content of mPP increases. Detailed T_c data of TPV and TPV/mPP/m-SiO$_2$ nanocomposites are listed on Ta-

TABLE II
T_m, T_c, and Thermal Stability of TPV/SiO$_2$ Nanocomposites

Sample	T_c (°C)	T_m (°C)	T_{onset} (°C)	$T_{-5\%}$ (°C)	$T_{-50\%}$ (°C)
TPV	93.3	136.1	247.5	303.9	404.1
TVS	94.4	136.3	262.4	310.1	417.3
TVSm1	96.0	149.0	264.7	309.4	411.2
TVSm3	99.9	151.5	264.1	309.9	413.7
TVSm5	103.9	153.2	265.7	311.9	412.9

ble II. This result indicates that the addition of functionalized compatibilizer mPP induces the crystal formation of the PP domain in TPV and further improves the interaction between TPV and m-SiO$_2$. Figure 4(b) shows the DSC heating curves of TPV and TPV/mPP/m-SiO$_2$ nanocomposites. The DSC results clearly show that the addition of only 1 wt % m-SiO$_2$ to the TPV matrix does not change its melting temperature (T_m), but T_m significantly shifts to higher temperatures as the content of mPP increases. Both X-ray and DSC data indicate that the addition of mPP is a usefully functionalized compatibilizer and can improve the interaction between m-SiO$_2$ and the TPV matrix.

Physical properties of the TPV/mPP/m-SiO$_2$ nanocomposites

The thermal stability of TPV/mPP/m-SiO$_2$ nanocomposites was measured by thermogravimetric analysis (TGA) in a nitrogen atmosphere. The TGA curves are shown in Figure 5. A summary of the TGA data is also given in Table II. Evidently, the onset temperature (T_{onset}) of the degradation of TPV/mPP/m-SiO$_2$ nanocomposites is 15–20°C higher than that of neat TPV. The 5% loss temperature ($T_{-5\%}$) and the 50% loss temperature ($T_{-50\%}$) of TPV/mPP/m-SiO$_2$ nanocomposites are also enhanced. This result shows that par-
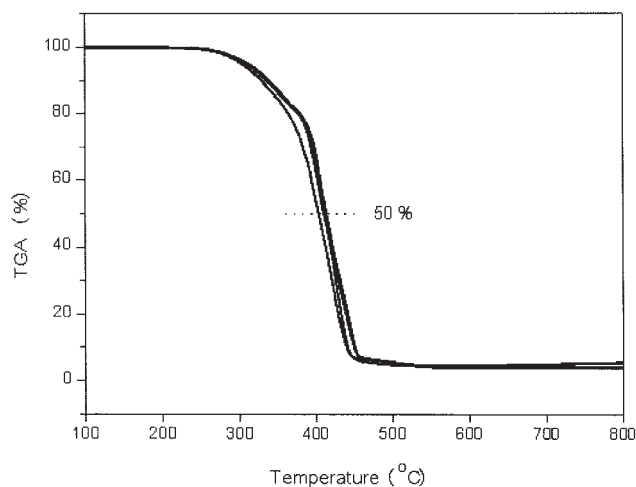

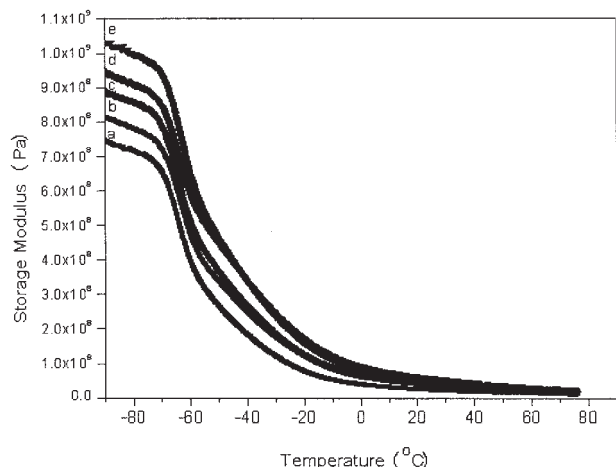**Figure 5** TGA curves for TPV and TPV/mPP/SiO$_2$ nanocomposites.

Figure 6 Storage modulus for (a) TPV, (b) TVS, (c) TVSm1, (d) TVSm3, and (e) TVSm5 nanocomposites.

tially introducing CTAB and mPP into the TPV/SiO$_2$ system can enhance the thermal stability of TPV/mPP/m-SiO$_2$ nanocomposites because of the better dispersion of m-SiO$_2$ and relatively strong interaction between m-SiO$_2$ and TPV in the TPV/mPP/m-SiO$_2$ nanocomposites.

Figure 6 shows the storage modulus of TPV and TPV/mPP/m-SiO$_2$ nanocomposites over a temperature range of −90 to 80°C. The data of the storage modulus at −90 and 30°C are listed in Table III. At −90°C, the storage modulus of TPV is 7.46×10^8 Pa, which decreases with increasing temperature; at 30°C, it drops to 0.22×10^8 Pa. This is attributed to insufficient thermal energy to overcome the potential barrier for transitional and rotational motions of segments of the polymer molecules in the glassy region, whereas above the glass-transition temperature (T_g), the thermal energy becomes comparable to the potential energy barriers to the segmental motions. It is clear from Figure 6 that the reinforcement effect is prominent above T_g of the PP phase (in the rubbery plateau) when the material is soft and flexible, and this causes a significant improvement in the storage modulus above T_g. At 30°C, the enhancement of the storage modulus (in comparison with that of virgin TPV) is 44.7% for TVS nanocomposites, 74.4% for TVSm1 nanocomposites, 118.7% for TVSm3 nanocomposites,

and 123.3% for TVSm5 nanocomposites. The enhancement of the storage modulus depends on the degree of dispersed m-SiO$_2$ nanoparticle and the content of functionalized compatibilizer mPP. This result is probably due to the presence of interactions between m-SiO$_2$ and TPV by functionalized compatibilizer mPP, which induces the crystalline formation of the PP domain in TPV. The polymer chains of semicrystalline PP that form the crystalline domain in TPV could be limited; partial PP/EPDM polymer chain motion and effective immobilization of these chains account for the increase in the hydrodynamic storage modulus.

The tensile strength and elongation at break obtained by tensile testing of the fabricated nanocomposites are listed in Table III. The tensile strength of all the TPV/mPP/m-SiO$_2$ nanocomposites is higher than that of pristine TPV. The addition of 1 wt % m-SiO$_2$ to TPV slightly improves the tensile properties. By the addition of the functionalized compatibilizer mPP, the enhancement of the tensile strength is 11.6% for TVSm1, 27.2% for TVSm3, and 32.8% for TVSm5. These results indicate that m-SiO$_2$ and mPP play important roles in the enhancement of the mechanical properties of TPV/mPP/m-SiO$_2$ nanocomposites. Table III also summarizes the adhesion strength obtained by the peeling test from the interface between the fabricated nanocomposites and stainless steel. The adhesion strength of all the TPV/mPP/m-SiO$_2$ nanocomposites is also higher than that of pristine TPV. The addition of 1 wt % m-SiO$_2$ to TPV slightly improves the interfacial adhesion. By the addition of the functionalized compatibilizer mPP, the enhancement of the adhesion strength is 20.1% for TVSm1, 39.6% for TVSm3, and 48.0% for TVSm5. These results indicate that the maleic anhydride group present in mPP plays an important role in adhesion with the interface of stainless steel.

CONCLUSIONS

TPV/mPP/m-SiO$_2$ nanocomposites have been successfully prepared by the melt blending of TPV and mPP into m-SiO$_2$ treated with CTAB as a grafting agent for TPV during the melt mixing. The thermal stability and storage modulus of a 1 wt % m-SiO$_2$ containing TPV/mPP/m-SiO$_2$ nanocomposite are sig-

TABLE III
Dynamic Mechanical Properties, Tensile Strength, and Adhesion Strength of TPV/mPP/m-SiO$_2$ Nanocomposites

Sample	Storage modulus (MPa)		Tensile strength (MPa)	Elongation at break (%)	Adhesion strength (MPa) to stainless steel
	−90°C	30°C			
TPV	746	21.9	87.4	278.6	16.2
TVS	812 (8.8%)	31.7 (44.7%)	93.5 (7.0%)	222.2 (−20.1%)	17.6 (9.2%)
TVSm1	891 (19.4%)	38.2 (74.4%)	97.5 (11.6%)	257.8 (−7.5%)	19.3 (20.1%)
TVSm3	948 (27.1%)	47.9 (118.7%)	111.2 (27.2%)	280.9 (0.9%)	22.5 (39.6%)
TVSm5	1003 (34.4%)	48.9 (123.3%)	116.1 (32.8%)	314.6 (12.9%)	23.8 (48.0%)

nificantly enhanced in comparison with that of pristine TPV. This result is probably due to the presence of interactions between m-SiO$_2$ and TPV by functionalized compatibilizer mPP, which induces the crystalline formation of the PP domain in TPV. The adhesion strength between TPV/mPP/m-SiO$_2$ nanocomposites and steel also increases with increasing m-SiO$_2$ content. With the addition of 1 wt % m-SiO$_2$ and functionalized compatibilizer mPP, the enhancement of the adhesion strength is 20.1% for TVSm1, 39.6% for TVSm3, and 48.0% for TVSm5. These results indicate that the maleic anhydride group present in mPP plays an important role in adhesion with the interface of stainless steel.

References

1. Giannelis, E. P. Adv Mater 1996, 8, 29.
2. Kojima, M.; Usuki, A.; Okada, A.; Kagimato, O. J Mater Res 1993, 8, 1185.
3. Wang, M. S.; Pinnavaia, T. J. Chem Mater 1994, 6, 468.
4. Graces, J.; Moll, D.; Bicerano, J.; Fibiger, R. Adv Mater 2000, 12, 1835.
5. Zheng, H.; Zheng, H.; Peng, Z.; Zhang, Y. Polym Test 2004, 23, 217.
6. Usuki, A.; Tukigase, A.; Kato, M. Polymer 2002, 43, 2185.
7. Zanetti, M.; Camino, G.; Canavese, D.; Morgan, A. B.; Lamelas, F.; Wilkie, C. A. Chem Mater 2002, 14, 189.
8. Liu, X.; Wu, Q. Polymer 2001, 42, 10013.
9. Yang, Y.; Chiba, T.; Saito, H.; Inoue, T. Polymer 1998, 39, 3365.
10. Kikuchi, Y.; Fukui, T.; Okada, T.; Inoue, T. Polym Eng Sci 1991, 31, 1029.
11. Ellul, M. D.; Patel, J.; Tinker, A. J. Rubber Chem Technol 1995, 68, 573.
12. Abdou-Sabet, S.; Puydak, R. C.; Rader, C. P. Rubber Chem Technol 1996, 69, 476.
13. Oldenbo, M. TPO-Nanocomposites for Automotive Exterior Bodypanels—Potential and Experience from Evaluation of Commercial Materials, Proceedings of Nanocomposites, Chicago, IL, June 25–27, 2001.
14. Mishra, J. K.; Kim, G.; Kim, I.; Chung, I.; Ha, C. J Polym Sci Part B: Polym Phys 2004, 42, 2900.
15. Liu, N. C.; Xie, H. Q.; Baker, W. E. Polymer 1993, 34, 4680.